Real-time dosimetry of proton microbeams at Birmingham’s MC40 cyclotron facility

Sophie Gibbins

Supervisor: Dr Tony Price
Project partner: Laurie Spoerer

Contents

Aims

Demonstrate feasibility of using a CMOS sensor for real-time beam measurements of proton microbeams at Birmingham’s MC40 cyclotron facility.

Investigate effect of PMMA bolus on beam characteristics.

Motivation

- Radiotherapy key aims:
  - deliver lethal dose to tumour
  - minimise healthy tissue damage
- Conventional radiotherapy performed with X-rays or electrons
- Protons have several advantages over X-rays
- Healthy tissue tolerates a higher dose when delivered via spatially fractionated radiotherapy
- CMOS sensor will allow real-time dosimetry

Proton interactions in matter

- Inelastic Coulomb scattering
- Elastic Coulomb scattering
- Nuclear interactions

- Beam diverges as it traverses matter
- Fluence decreases

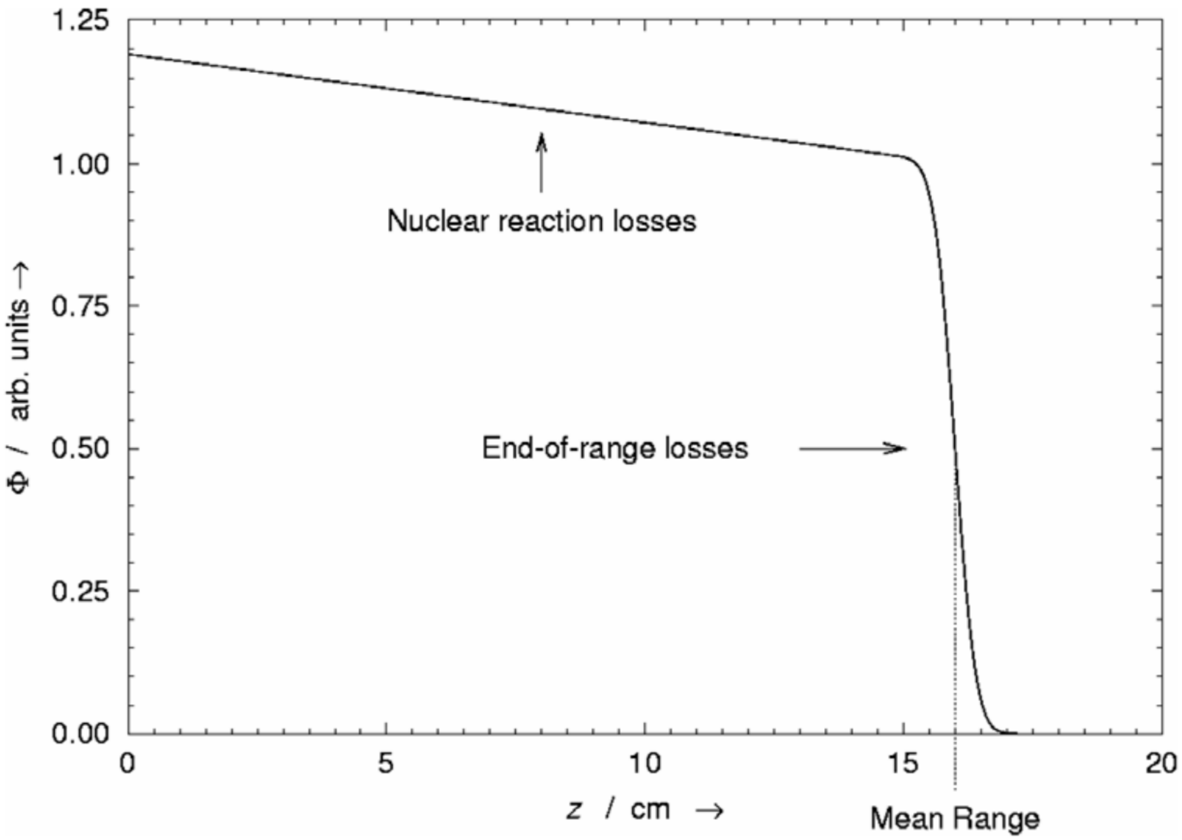

Fig 1. Proton fluence as a function of depth in water with mean range, the depth where half the initial protons have been absorbed, highlighted [1].

[1] Wayne D Newhauser and Rui Zhang. The physics of proton therapy. Physics in Medicine and Biology, 60(8):R155–R209, Mar 2015.

Why protons?

- Dose deposited is inversely proportional to the square of the proton velocity
- Maximum dose deposited at Bragg peak
- Sharp distal fall-off following Bragg peak
- Tissue sparing - key aim of radiotherapy

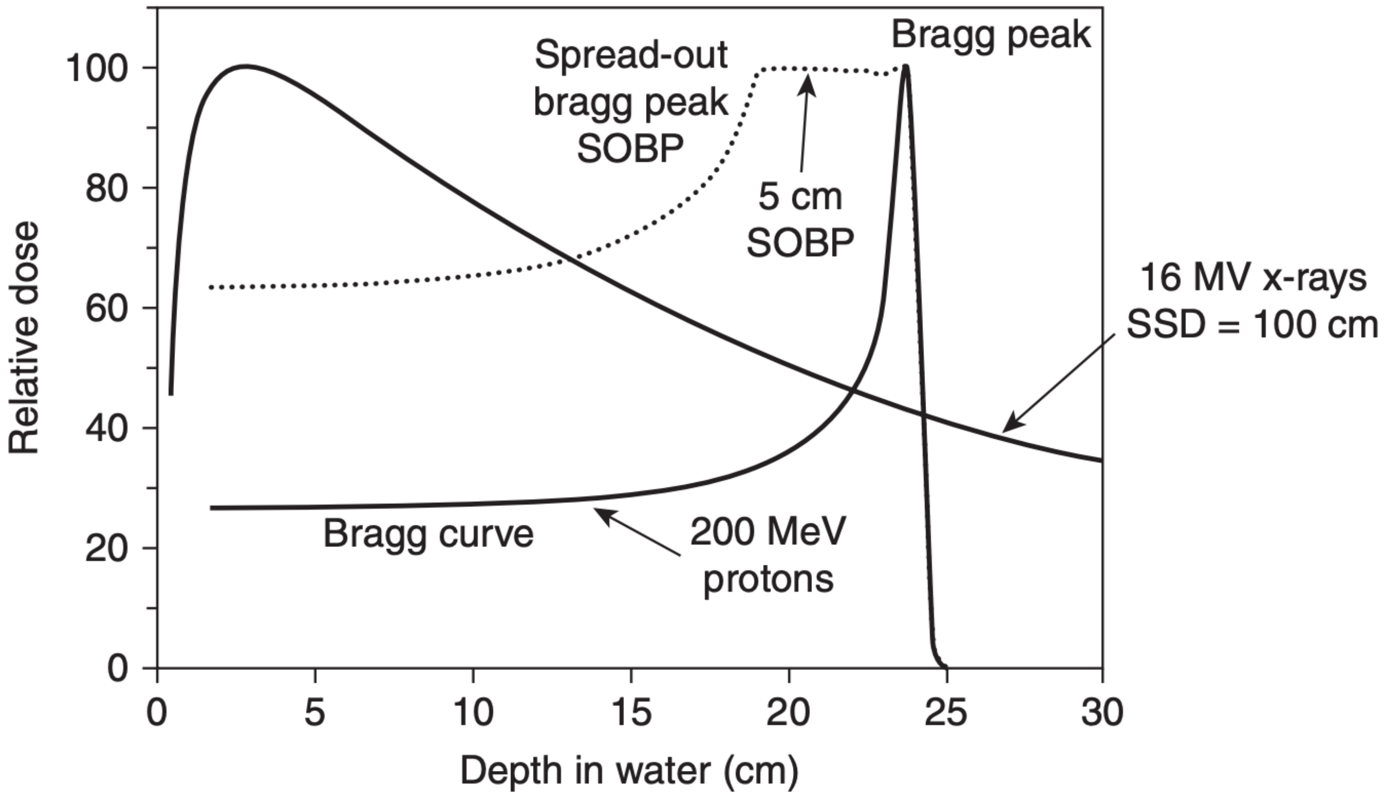

Fig 2. Depth dose comparison for 16MV X-ray beam and 200MeV proton beam in a 10x10cm^2 field [2].

[2] Frank S.J and Zhu X. R. Chapter 2 - principles of proton beam therapy. In Proton Therapy, pages 14–24. Elsevier, Philadelphia, 2021.

Microbeam radiotherapy

- Parallel, spatially fractionated beams tens of microns wide
- Beams delivered from multiple angles
- Healthy tissue tolerates a higher dose [3]
- Peak-to-valley dose ratio (PVDR) key metric

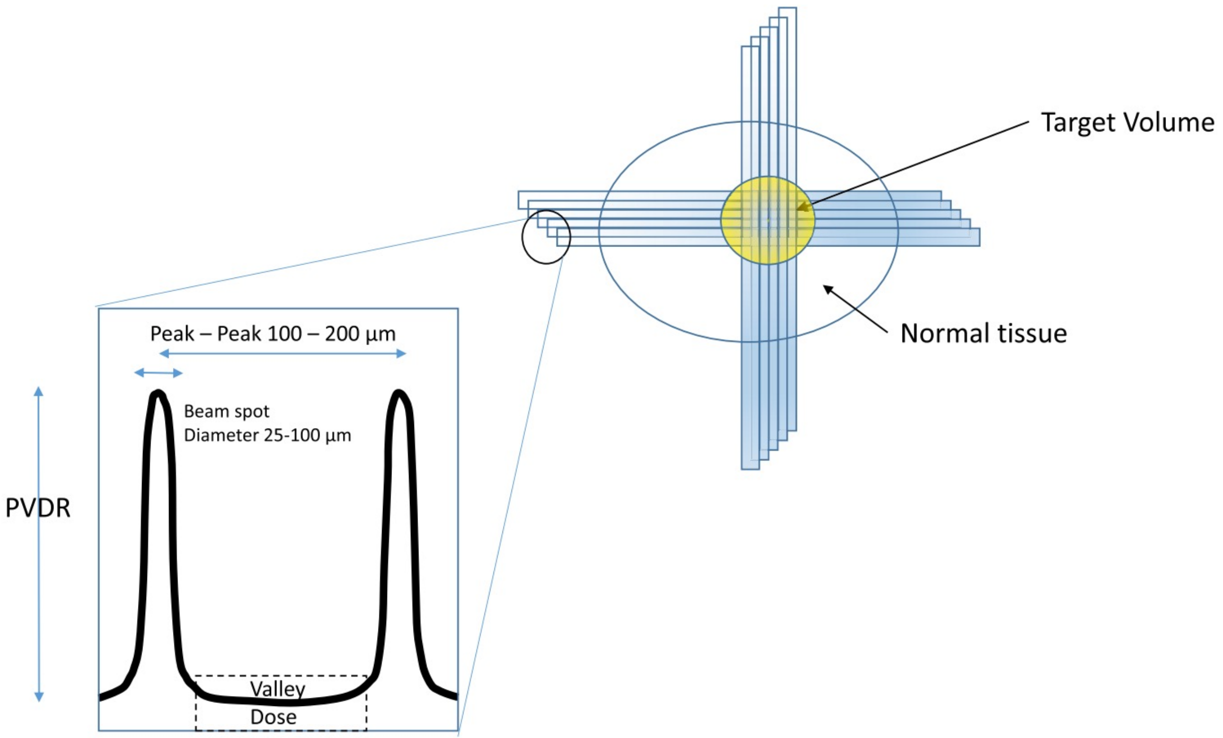

Fig 3. Schematic diagram of two beams forming a lattice over the target volume with a profile highlighting the PVDR [4].

[3]O. Zlobinskaya, S. Girst, C. Greubel, and et al. Reduced side effects by proton microchannel radiotherapy: study in a human skin model. Radiat Environ Biophys, 52:123–133, 2013.
[4] H. Fukunaga, K.T. Butterworth, S.J. McMahon, K.M. Prise. A Brief Overview of the Preclinical and Clinical Radiobiology of Microbeam Radiotherapy. Clinical Oncology. 2021; 33(11): 705-712

Proton Microbeam Radiotherapy (pMRT)

- Spatially fractionate protons to achieve homogeneous dose at tumour site
- Advantageous for radioresistant tumours/tumours close to critical structures

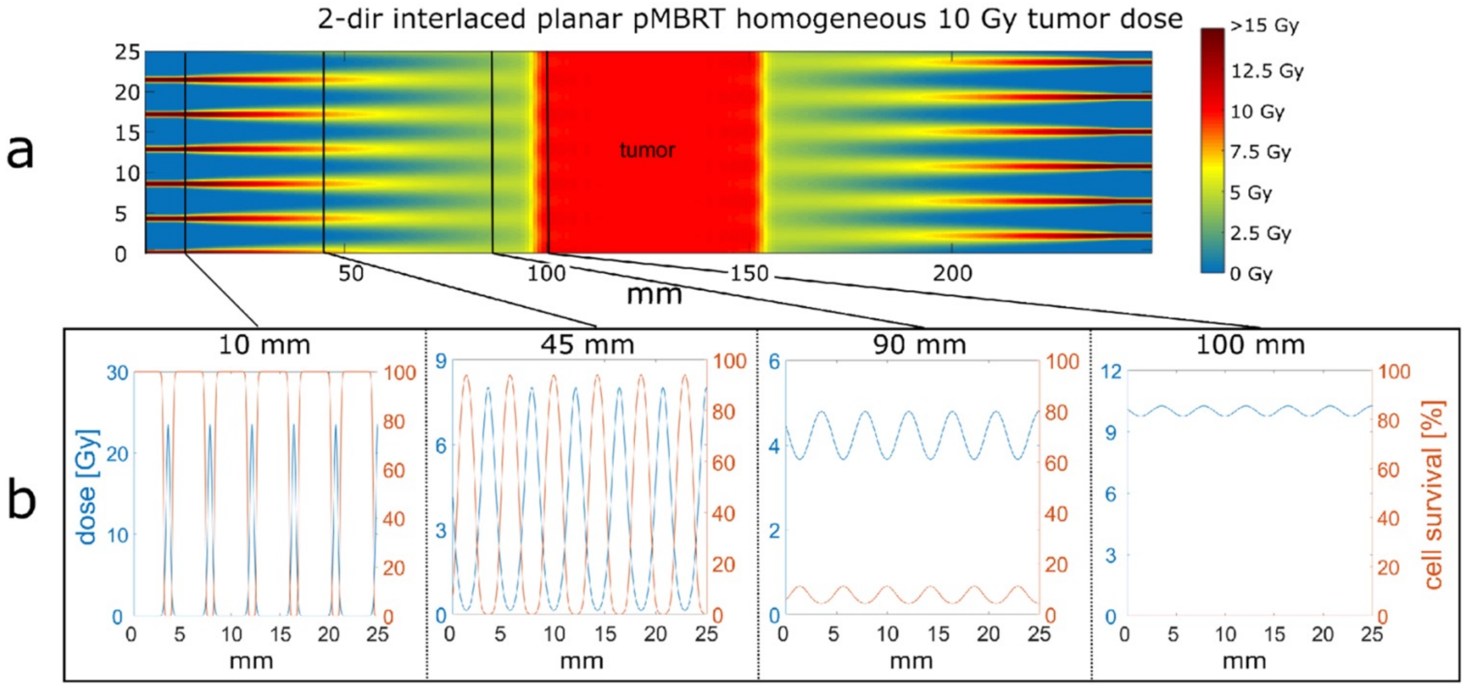

Fig 4. a) Proton minibeam dose map showing homogeneous tumour dose and b) beam cross-section at several depths highlighting dose and clonogenic cell survival [5].

[5] Sammer, M., Girst, S. & Dollinger, G. Optimizing proton minibeam radiotherapy by interlacing and heterogeneous tumor dose on the basis of calculated clonogenic cell survival. *Sci Rep* **11,** 3533 (2021). https://doi.org/10.1038/s41598-021-81708-4

LASSENA sensor

- Current methods for x-ray microbeams involve GafChromic film – takes days to develop
- Complementary metal-oxide-semiconductor (CMOS) sensor allows for real-time beam measurements
- PN junction results in a depletion layer
- Protons ionize silicon, electrons are collected at the N-well
- Successfully used for x-ray microbeam measurements [6]

[6] Samuel Flynn, Tony Price, Philip P. Allport, Ileana Silvestre Patallo, Russell Thomas, Anna Subiel, Stefan Bartzsch, Franziska Treibel, Mabroor Ahmed, Jon Jacobs-Headspith, Tim Edwards, Isaac Jones, Dan Cathie, Nicola Guerrini, and Iain Sedgwick. First demonstration of real-time in-situ dosimetry of x- ray microbeams using a large format cmos sensor. Nuclear Instruments and Methods in Physics Research Section A: Accelerators, Spectrometers, Detectors and Associated Equipment, 978:164395, 2020.

Project outline

- Measurements made at Birmingham’s MC40 cyclotron with 36MeV proton beam
- Scattered, collimated beam
- Experiments:
  - Current calibration
  - PVDR at varying distance in air
  - Measurements through increasing depth of PMMA
  - GafChromic film at 0mm, 3mm and 7mm in air and 3mm in PMMA

Collimators

- Ta, 2mm thick, 100µm slit width, 500µm c-t-c spacing
- Measured using SmartScope in clean rooms

Collimator	Slit width (µm)	Slit spacing (µm)
1	102 ± 4	399 ± 2
2	127 ± 5	372 ± 7

Table 1. Mean slit widths and spacing of each Ta collimator.

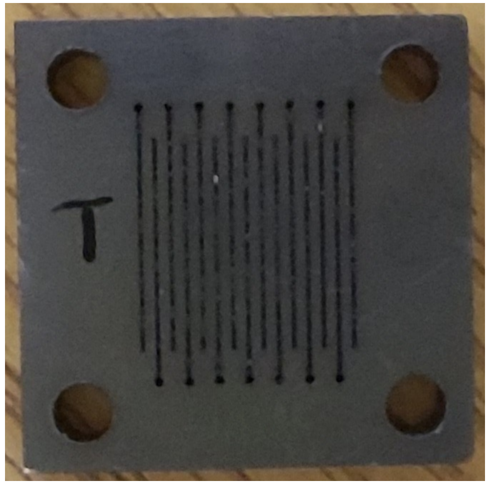

Fig 5. Tantalum collimator.

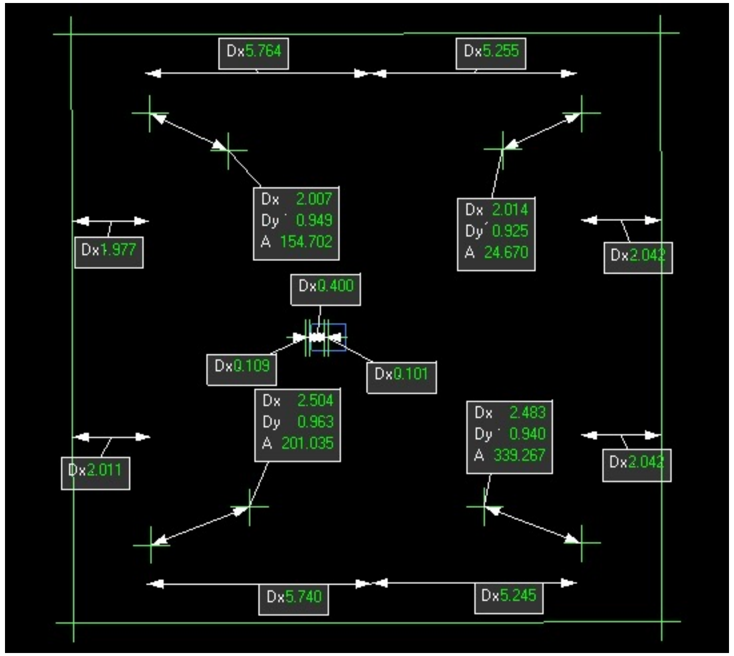

Fig 6. Schematic of measurements made with SmartScope.

Calibration

- $2x2cm^2$ field size
- Sensor at nominal 0mm
- Charge and integration time recorded
- Dark frames taken periodically
- Separate measurements with Markus chamber

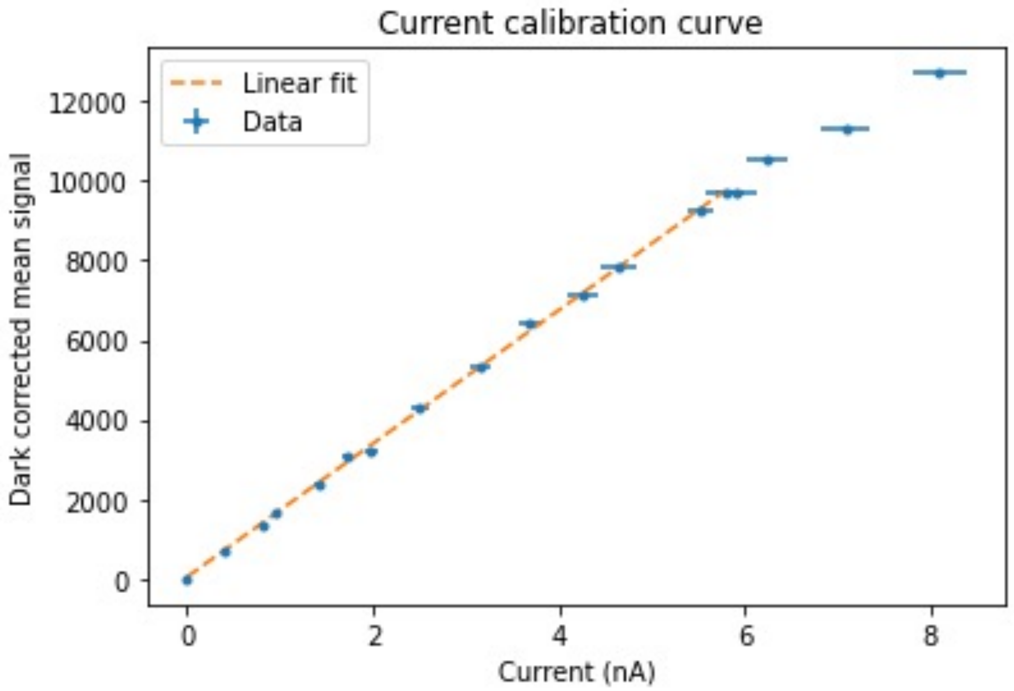

Fig 8. Current calibration curve with a linear fit to data points below 10000 digital units.

Fig 7. Set-up for taking calibration data.

Air measurements: set-up

- 2 collimators
- At nominal 0mm position sensor face approx. 1mm from collimator
- Sensor moved back in steps of 1mm
- Measurements repeated over both experimental days

a

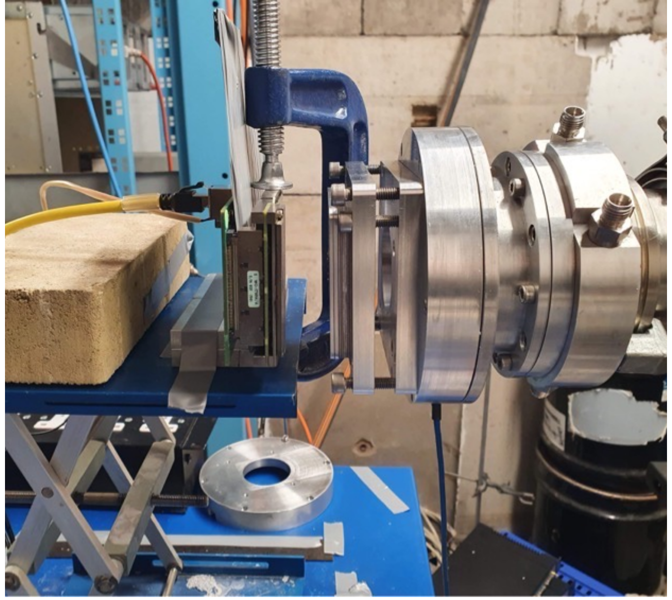

b

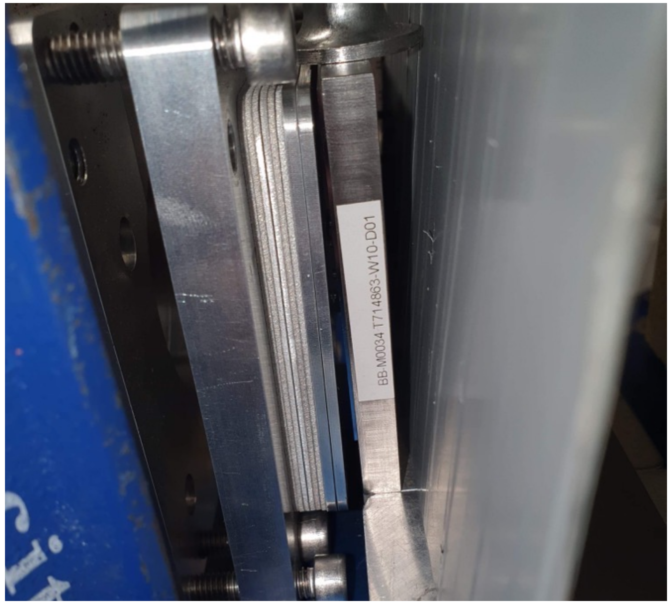

c

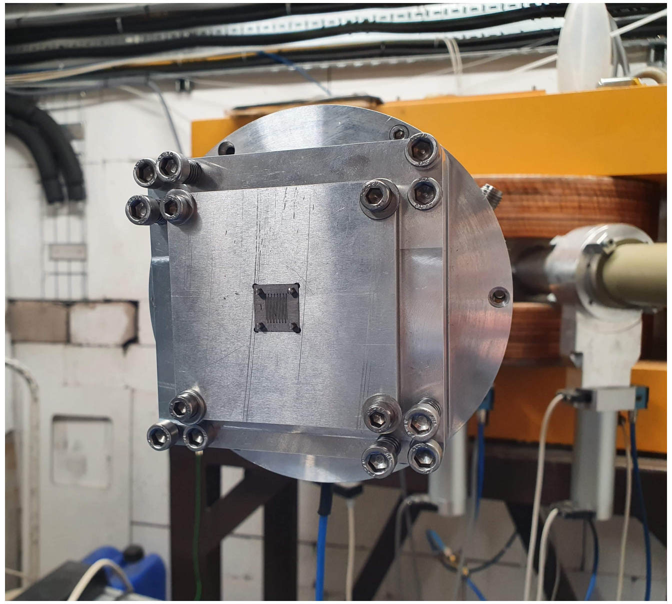

d

Fig 9. Pictures showing a) sensor face, b) set-up with rulers, c) gap between collimator and sensor face at 0mm and d) collimator on end of beam-line.

Air measurements: results

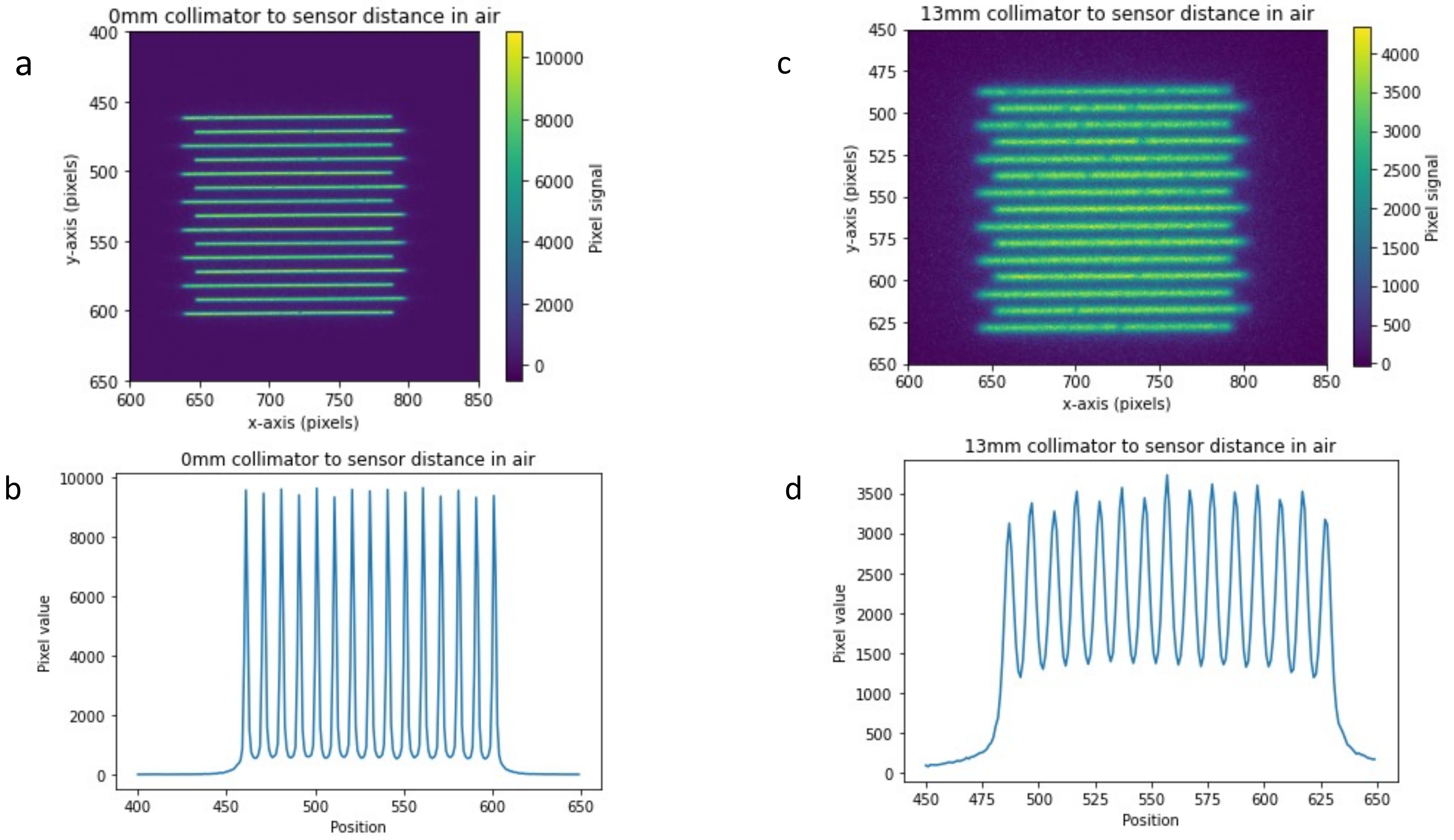

Fig 10. Beam image at a) 0mm and c) 13mm with corresponding profiles (b) and (d) of signal value averaged across 100 columns.

Air measurements: results (2)

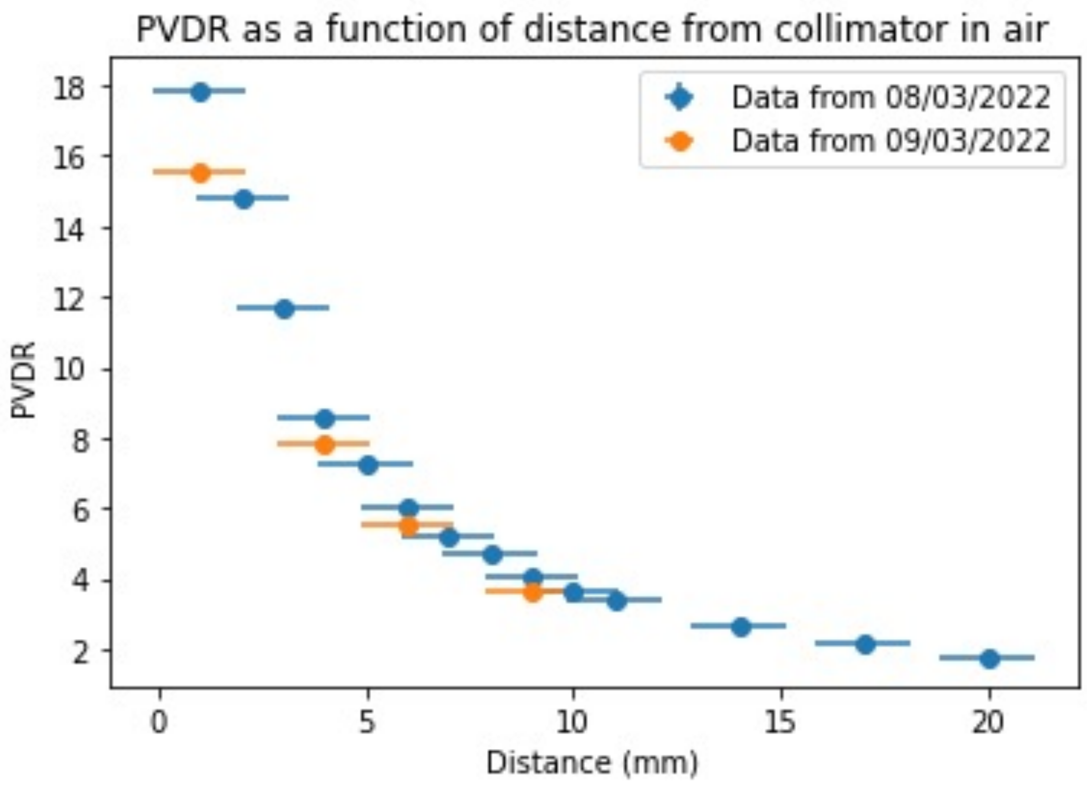

Fig 11. PVDR as a function of distance in air from the collimator measured on consecutive days.

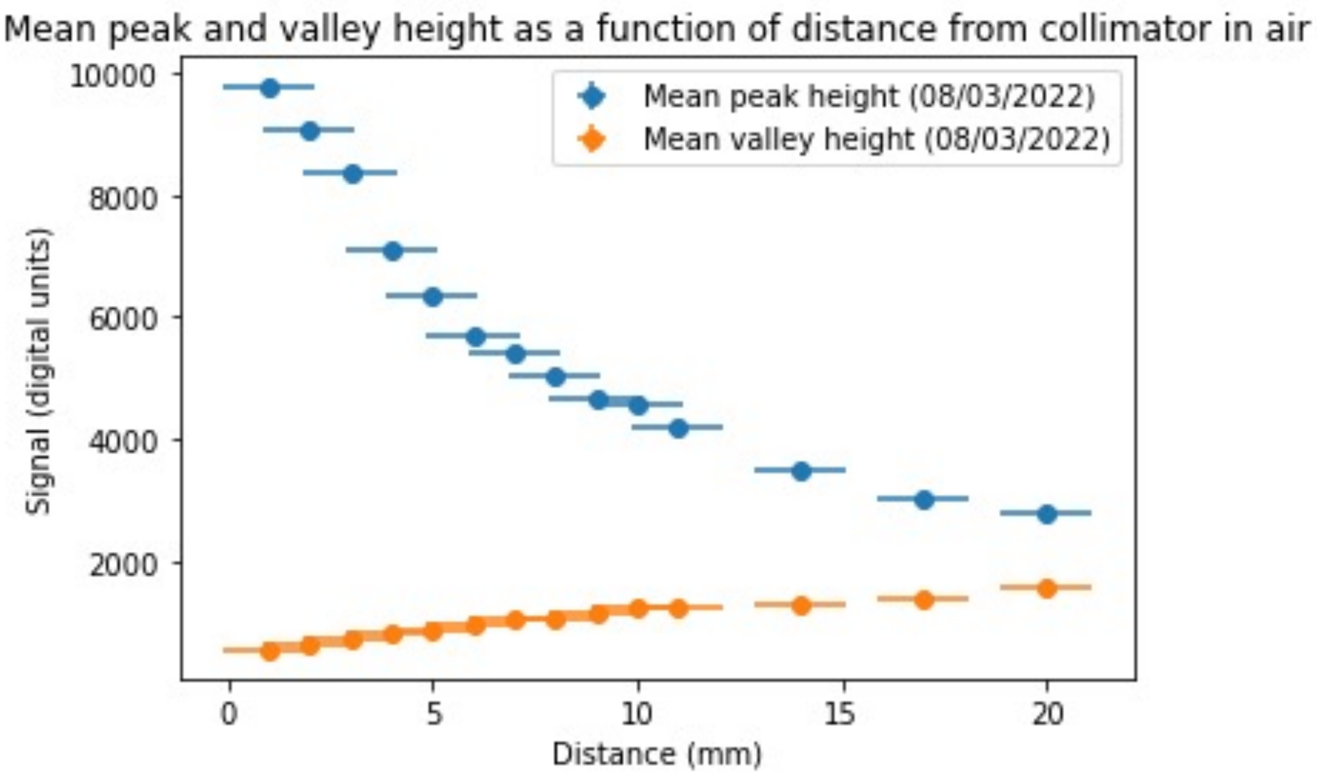

Fig 12. Mean peak and valley heights as a function of distance in air from the collimator.

PMMA measurements: Set-up

- 2 collimators
- PMMA of increasing thickness taped to front of collimator
- Detector moved forward to corresponding position on ruler so that there was no air gap between detector and PMMA
- Charge and integration time recorded to account for fluctuations of beam current

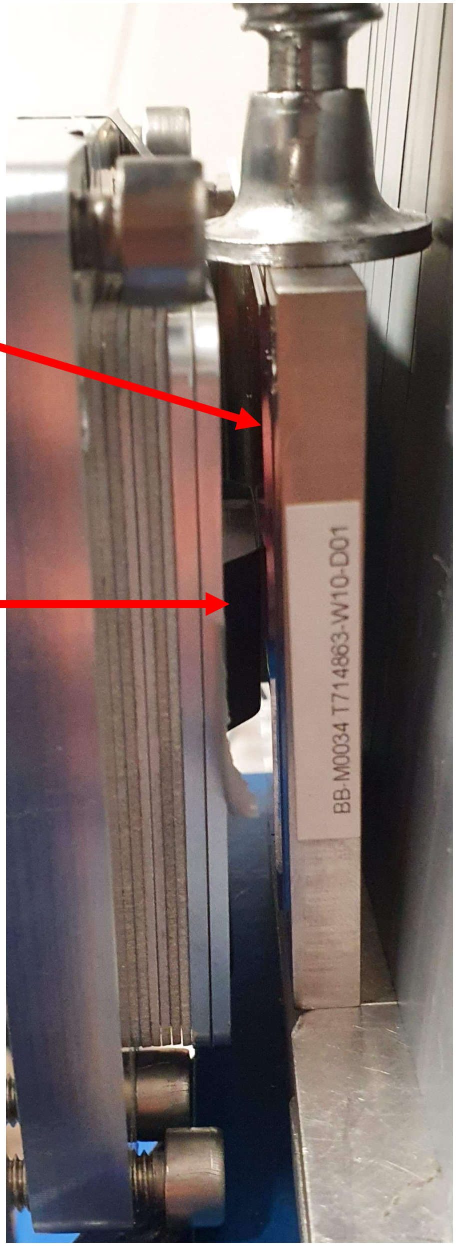

Fig 13. Set-up with PMMA in place and in contact with sensor face.

PMMA measurements: results (1)

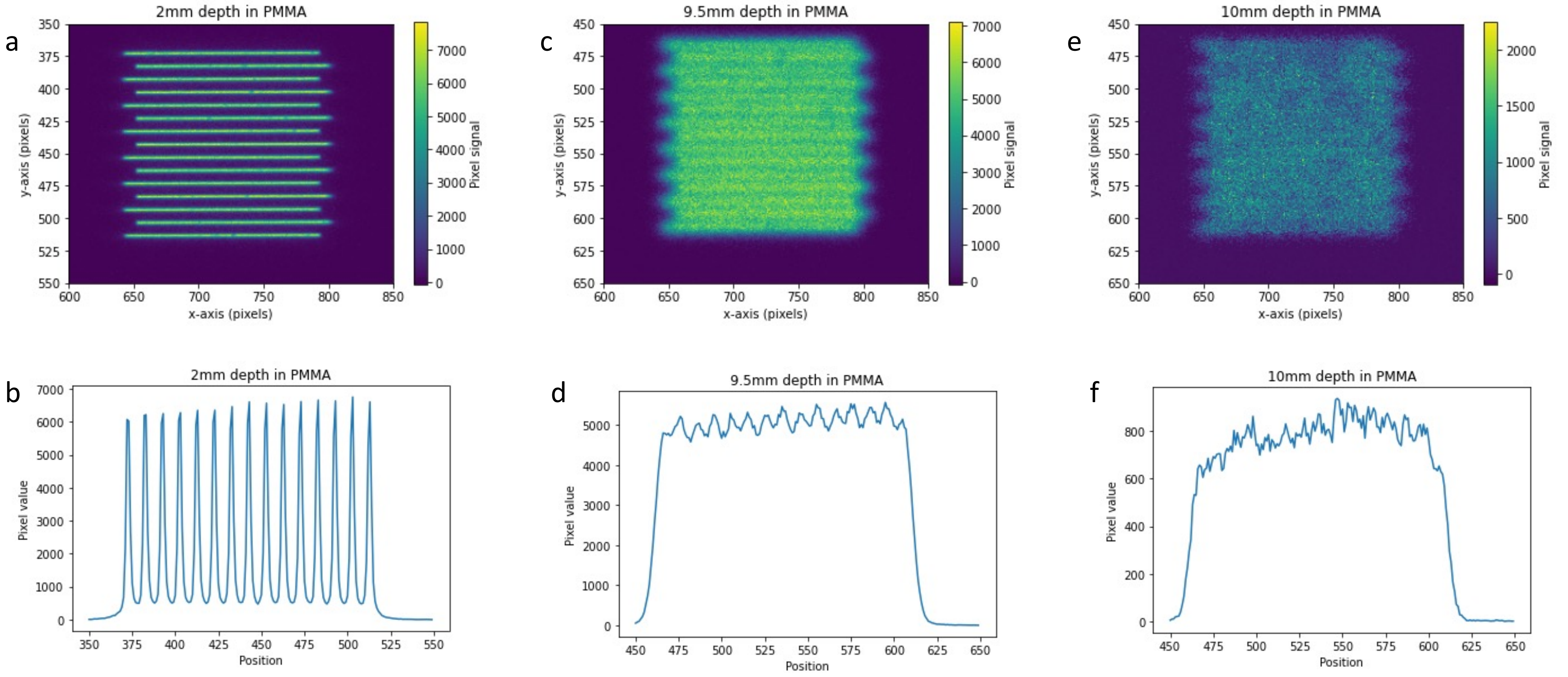

Fig 14. Images of the beam at a) 2mm, c) 9.5mm and e) 10mm depth in PMMA. Corresponding profiles of the pixel signal averaged across 100 columns are shown in b), d) and f).

PMMA measurements: results (2)

- Shape of curve a combination of proton scattering and increased stopping power
- PVDR at 3mm depth in PMMA 9.97±0.08 compared with MC simulation 9.1±0.1

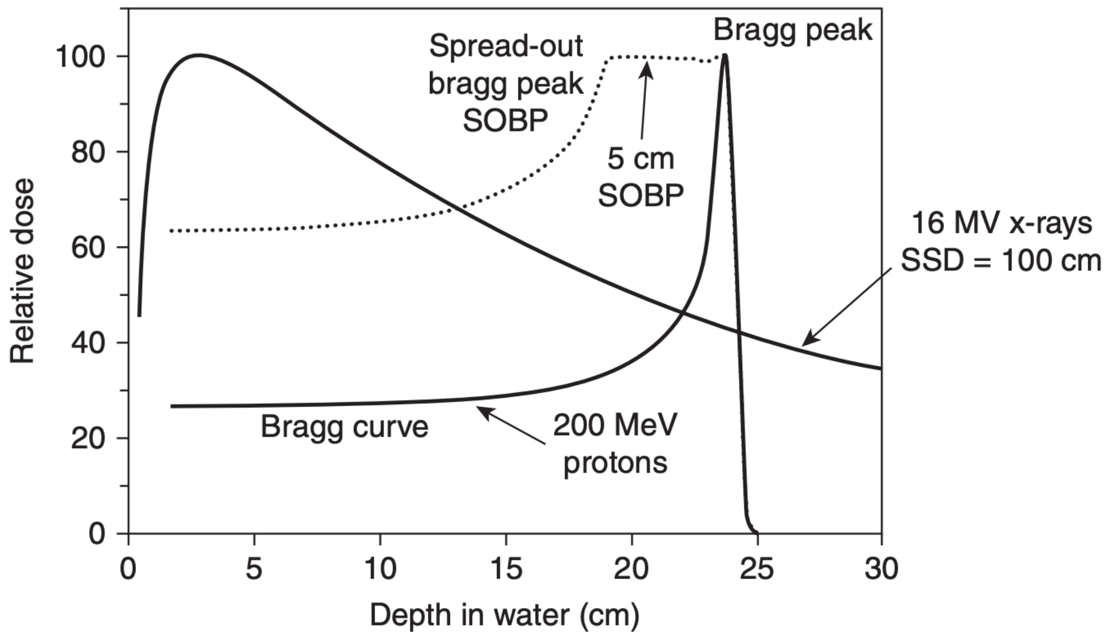

Fig 15. Depth dose comparison for 16MV X-ray beam and 200MeV proton beam in a 10x10cm^2 field [2].

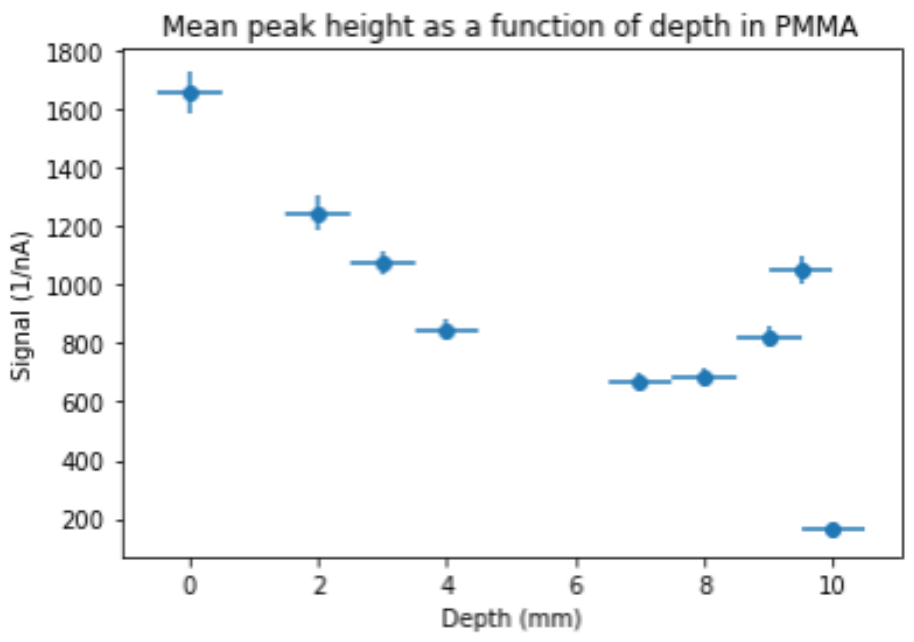

Fig 16. Mean signal normalized to current value as a function of depth in PMMA.

[2] Frank S.J and Zhu X. R. Chapter 2 - principles of proton beam therapy. In Proton Therapy, pages 14–24. Elsevier, Philadelphia, 2021.

Next steps

- Refine code for data fitting
- Dose conversion
- Analyse Monte-Carlo simulation data for PMMA
- Compare simulations with results
- Compare with film results

Summary

- CMOS sensor allowed real-time beam measurements
- PVDR comparable with proton minibeam PVDR measured at Institut Curie Proton Therapy Center [7]
- Scattering in air significantly decreased PVDR
- Bragg peak and distal fall-off witnessed in PMMA
- PMMA simulation data comparable with results
- Continue analysis of experimental and simulation data and compare with film dosimetry

[7] Peucelle C, Nauraye C, Patriarca A, Hierso E, Fournier-Bidoz N, Mart́ ınez-Rovira I, and Prezado Y. Proton minibeam radiation therapy: Experimental dosimetry evaluation. Med Phys, 42(12):7108–13, 2015.